Ultrasound in Med. & Biol., Vol. 47, No. 12, pp. 3501–3513, 2021
Copyright © 2021 The Author(s). Published by Elsevier Inc. on behalf of World Federation for Ultrasound in Medicine & Biology.
This is an open access article under the CC BY license (http://creativecommons.org/licenses/by/4.0/)
Printed in the USA. All rights reserved.
0301-5629/$ - see front matter

https://doi.org/10.1016/j.ultrasmedbio.2021.08.021

● *Original Contribution*

INTRAVENTRICULAR VECTOR FLOW IMAGING WITH BLOOD SPECKLE TRACKING IN ADULTS: FEASIBILITY, NORMAL PHYSIOLOGY AND MECHANISMS IN HEALTHY VOLUNTEERS

ANNICHEN SØYLAND DAAE,*,† MORTEN SMEDSRUD WIGEN,* SOLVEIG FADNES,*,‡ LASSE LØVSTAKKEN,* and ASBJØRN STØYLEN*,†

* Department of Circulation and Medical Imaging, Norwegian University of Science and Technology, Trondheim, Norway; † Department of Cardiology, St. Olav Hospital/Trondheim University Hospital, Trondheim, Norway; and ‡ Møre og Romsdal Hospital Trust, Women's Health, Child and Adolescent Clinic, Ålesund Hospital, Ålesund, Norway

(*Received* 17 *February* 2021; *revised* 24 *August* 2021; *in final form* 29 *August* 2021)

Abstract—This study examines the feasibility of blood speckle tracking for vector flow imaging in healthy adults and describes the physiologic flow pattern and vortex formation in relation to the wall motion in the left ventricle. The study included 21 healthy volunteers and quantified and visualized flow patterns with high temporal resolution down to a depth of 10–12 cm without the use of contrast agents. Intraventricular flow seems to originate during the isovolumetric relaxation with a propagation of blood from base to apex. With the E-wave, rapid inflow and vortex formation occurred on both sides of the valve basally. During diastasis the flow gathers in a large vortex before the pattern from the E-wave repeats during the A-wave. In isovolumetric contraction, the flow again gathers in a large vortex that seems to facilitate the flow out in the aorta during systole. No signs of a persistent systolic vortex were visualized. The geometry of the left ventricle and the movement of the AV-plane is important in creating vortices that are favorable for the blood flow and facilitate outflow. The quantitative measurements are in concordance with these findings, but the clinical interpretation must be evaluated in future clinical studies. (E-mail: annichen.s.daae@ntnu.no) **© 2021 The Author(s). Published by Elsevier Inc. on behalf of World Federation for Ultrasound in Medicine & Biology. This is an open access article under the CC BY license (http://creativecommons.org/licenses/by/4.0/).**

Key Words: **Ultra high frame rate, Vortex imaging, Kinetic energy, Energy loss, Vorticity, Intraventricular pressure difference, Intraventricular pressure gradient.**

INTRODUCTION

Already in 1972, Bellhouse (1972) described the fluid mechanics of a model mitral valve and the left ventricle (LV). In 1990 Bot et al. (1990) described a vortex ring in a model of the LV and concluded that the size of the ventricle is a determinant of the vortices. In 1994 Steen and Steen (1994) described the flow pattern in the LV by the use of a model LV and color M-mode (CMM) echocardiography. They described initial diastolic flow propagation moving fast toward the apex of the LV and the subsequent vortex propagation, which moves slower. In 1995 Kim et. al. (1995) used cardiac magnetic resonance imaging (CMR) to map and describe the normal flow pattern in the LV for the first time, describing the large anterior vortex that emerges during mitral inflow. In the same year, Bohs et al. (1995) did a phantom *in vitro* test of speckle tracking for direction independent visualization of blood flow velocities. The Doppler technology only shows uni-directional flow and cannot obtain velocity estimates perpendicular to the beam direction, and thus several different ultrasound techniques for determination of flow velocities perpendicular to the ultrasound beam have been described. The different methods used for vector flow imaging (VFI) are thoroughly explained by Jensen et al. (2016a, 2016b), where echo particle image velocimetry (echo-PIV) (Cimino et al. 2012), vector flow mapping (VFM) (Garcia et al. 2010) and blood speckle tracking (BST) are the most commonly pursued methods for cardiac VFI. In conventional 2-D flow imaging, temporal resolution has been low; thus, the details of the short-lived isovolumetric phases, as well as the relation of the vortices created during early and late filling, have not been

Correspondence to: Annichen Søyland Daae, Norwegian University of Science and Technology Faculty of Medicine and Health Sciences, Trondheim, Norway. E-mail: annichen.s.daae@ntnu.no

described in detail. Together with the evolution of the VFI field, the energy loss (EL) (Zhong et al. 2016; Akiyama et al. 2017; Elbaz et al. 2017; Xu et al. 2017), the kinetic energy (KE) (Arvidsson et al. 2013; Kanski et al. 2015; Akiyama et al. 2017) and the concept of vorticity (VO) have been described (Hong et al. 2008; Mehregan et al. 2014; Pedrizzetti et al. 2014; Fenster et al. 2015), but the methods used to extract the measurements differ.

Combining high-frame-rate/ultra-fast ultrasound imaging and BST provides new opportunities for the estimation and visualization of 2-D and 3-D blood velocities (Van Cauwenberge et al. 2016; Fadnes et al. 2017; Wigen et al. 2018), which were recently used in research within pediatric echocardiography (Nyrnes et al. 2020). With the BST method, we can visualize the flow patterns qualitatively and extract the quantitative measurements rate of ĖL, KE, VO and the intraventricular pressure difference (IVPD) (Fadnes et al. 2020). Also, with the unique acquisition method described by Wigen et al. (2018), we get ultra-high temporal resolution. Using BST in adults is more challenging than in children because imaging in adults must reach deeper into the body. To increase the depth, a probe with a lower frequency is used; a lower frequency will, in turn, lead to a reduced spatial resolution both laterally and in depth. This is required for an increased depth with less attenuation in the deeper parts of the image. This study describes the first clinical results of BST for VFI in healthy adults.

The first aim of this study was to demonstrate the feasibility of BST for VFI in healthy adults. The second aim was to use the BST method to visualize and describe the physiologic flow pattern and vortex formation with relation to the wall motion throughout the entire cardiac cycle in the healthy LV.

METHODS

Study population

This study included 23 healthy volunteers; two were excluded, one because of frequent extra systoles and one because of a technical error in electrocardiography (ECG) recording, both making ECG stitching of images unfeasible. The remaining 21 subjects were included for further analysis. No subjects were excluded because of poor image quality. The study was approved by the regional ethics committee, and all subjects signed an informed consent form. The subject characteristics are listed in Table 1.

Table 1. Characteristics of the subjects (n = 21)

Age (y)	33 (25−68)
Sex (men/women)	16/5
Systolic blood pressure (mmHg)	129 (118−135)
Diastolic blood pressure (mmHg)	84 (77−90)
Height (cm)	177 (171−180)
Weight (kg)	72 (69−83)
Body mass index	23 (21−27)
Heart rate (beats/min)	64 (59−73)

Data are expressed as median (interquartile range) or number, except for age, which is expressed as number (range).

Standard echocardiography

The examination was performed with a GE E95 ultrasound scanner (GE Vingmed, Horten, Norway), using the M5S-c probe in the left lateral decubitus position. Standard echocardiographic data were acquired from both the parasternal and the apical views and consisted of standard B-Mode cine loops with and without color Doppler imaging (CDI), continuous-wave (CW) Doppler, pulsed-wave (PW) Doppler, tissue Doppler imaging (TDI) and CMM. The standard echocardiographic recordings were transferred for off-line analysis in a designated work package (EchoPAC BT 203, GE Vingmed, Horten, Norway). All images were obtained by, or under supervision of, a senior cardiologist with significant echocardiography experience.

Ejection fraction (EF) was measured by the modified Simpsons method in the apical four-chamber and long axis view, with the automated function in EchoPAC. Mitral annular plane systolic excursion (MAPSE) was measured by reconstructed M-mode through the mitral annulus in the apical four-chamber view and averaged for the inferoseptal and anterolateral points. Peak velocities from the mitral valve and the LVOT and spectral tissue Doppler mitral annular velocities were recorded and measured as described by the American Society of Echocardiography (ASE) and the European Association of Cardiovascular Imaging (EACVI) (Nagueh et al. 2016). The spectral tissue Doppler velocities from the mitral annulus (s', e' and a') are averaged from the septal and lateral values. Flow propagation velocity is measured in the CMM images by a straight line drawn in the front of the aliased velocity.

The isovolumetric relaxation (IVR) interval was measured from aortic valve closure (AVC) to mitral valve opening (MVO) in Doppler recordings and transferred to color tissue Doppler cycles automatically by the analysis software. Strain rate was measured by tissue Doppler in the middle of the IVR as the average of three cycles, and in four points (septal and lateral apical and basal) (Supplementary Fig. 1). One subject was excluded because of extensive clutter noise in the TDI recordings and one partially because of angulation error in the lateral base. Three subjects had less than three full cycles.

VFI

VFI in this study is done with our in-house developed method called BST. The examination was

performed with a GE E95 ultrasound scanner (GE Vingmed, Horten, Norway) using the 4V-D probe. High-frame-rate data were obtained from the setup described by Wigen et al. (2018), where a combination of plane wave emission and multi-beat ECG stitching was used to obtain continuous data acquisition (>3500 frames/s). By using the 3-D probe and multiple line acquisition, a 3-D slice of 10 degrees was obtained from a 2-D preview. Five to six beats were used for high-frame-rate data, and two beats for high-quality B-mode images. The acquired 3-D data underwent wall filtering using singular value decomposition (Yu and Lovstakken 2010; Demené et al. 2015) by excluding the 1000 first eigenvectors. BST was performed on the filtered data according to Wigen et al. (2018) and averaged over 15 frames. The same data were also used to process CDI. The processed data were displayed as a 2-D image with a temporal resolution of >233 frames/s.

Further, the raw blood velocity data were post-processed with a model-based regularization scheme developed by Grønli et al. (2018), which is also described in clinical work by Nyrnes et al. (2020). A regularized velocity field was acquired by combining a manually annotated endocardium with a fluid model, defined by the Navier-Stokes equation. The objective of this last processing step was to reduce noise in the measurements, which are sensitive to unnatural irregularities in the flow field, as well as to fill in empty values in regions without BST estimates owing to signal loss caused by wall filtering. The cine loops were also marked with systole and diastole. End of systole was defined as the time when the AV-plane stopped moving after ejection. End of diastole was defined as the time when the mitral valve was closed after the A-wave. This means that the isovolumic contraction (IVC) period is at the start of systole, while the IVR is at the start of diastole.

The BST data allow for the measurement of quantitative flow properties, such as KE, ĖL and VO. KE is the energy the blood possesses owing to its motion, while ĖL is related to the viscous losses of the fluid. Both are studied as markers for an effective intraventricular blood flow (Kanski et al. 2015; Wang et al. 2016; Zhong et al. 2016; Nakashima et al. 2017). VO is related to the rotation of the blood at one timepoint in the cardiac cycle and is a measure of the complexity of the blood flow. BST also allows for the measurements of IVPD because pressure and flow are linked through the Navier-Stokes equations. The pressure gradients are calculated based on the BST velocity field, and the base-to-apex pressure difference is found by integrating the gradients along a manually defined path. The path is a spline curve defined by three or more points set by the user according to the mitral inflow streamlines. The IVPD is measured throughout the cardiac cycle, but because the path is static and drawn in IVR/early diastole, the values are most precise during this time. The IVPD in the IVR is measured shortly before the opening of the mitral valve. The maximum IVPD at the rapid inflow is measured just before the first aliasing (*i.e.*, the start of the highest velocity) of the E-wave. In three of the subjects, we had poor visualization of the mitral flow and could therefore not place the path correctly. These three subjects are excluded from the analyses of IVPD. Definitions, equations and a more thorough explanation of the quantitative measures can be found in the appendix.

Statistical analysis

The data are presented as number or median (interquartile range) because the sample of 21 subjects was not normally distributed. Data were plotted in an SPSS worksheet and were later analyzed using IBM SPSS Statistics version 25.0 (IBM, Armonk, NY, USA) and with Python using the Statsmodels package for analyses and the Seaborn library for visualization.

RESULTS

Conventional echocardiographic findings are shown in Table 2. The measurements were well within normal values and showing normal age differences. The BST method was able to visualize and quantify flow patterns in all included subjects.

Qualitative flow results

Throughout the cardiac cycle a vortex that is visible during most of the cycle is observed. The vortex has a counterclockwise direction in the apical four-chamber view and a clockwise direction in the apical long axis view with standard orientations (*i.e.,* rotation toward the left ventricular outflow [LVOT]). Thus, it facilitates the movement of blood from the mitral orifice toward the

Table 2. Echocardiographic characteristics of subjects (n = 21)

EF (%)	54 (52–62)
MAPSE (mm)	16 (14 – 17)
Peak velocity E (m/s)	0.82 (0.65–1.00)
Peak velocity A (m/s)	0.56 (0.47–0.68)
Deceleration time E (ms)	153 (123–182)
E/A ratio	1.53 (1.03–1.87)
E/e'	5.50 (4.95–7.65)
Peak velocity s' (m/s)	0.10 (0.09–0.11)
Peak velocity e' (m/s)	0.14 (0.12–0.18)
Peak velocity a' (m/s)	0.08 (0.07–0.10)
Peak velocity LVOT outflow (m/s)	1.03 (0.95–1.09)
Flow propagation velocity E CMM (cm/s)	66 (62–92)

Data are expressed as median (interquartile range).

CMM, color M-mode; EF, ejection fraction; LVOT, left ventricular outflow tract; MAPSE, mitral annular plane systolic excursion; s', systolic tissue velocity; e', early diastolic tissue velocity; a', late diastolic tissue velocity; E, early filling; A, atrial contraction/late filling.

aortic valve (Kilner et al. 2000; Cimino et al. 2012; Pedrizzetti et al. 2014; Li et al. 2019).

Figure 1 show the different phases in the cardiac cycle seen with the ECG and the vector plots. The visual impression of this method is better when viewed as a video compared with still images, and Supplemental Videos 1–4 demonstrate the same flow pattern as Figure 1 and the following description.

The first sign of intraventricular movement of the blood is seen in the IVR as a low-velocity flow from the basis toward the apex in the CDI (Fig. 1a). This low-velocity flow is visible with both the mitral and the aortic valve closed. An elongation in the apex and shortening in the base can be demonstrated during IVR with strain rate curved anatomical M-mode (CAMM) (Suppl. Fig. 1). This concept of start of flow has been demonstrated earlier (Sasson et al. 1987; Garcia et al. 2010; Cimino et al. 2012). During early rapid filling (E), the AV-plane moves away from the apex, expanding the LV. Along with the rapid column of blood flowing into the LV during this phase, the flow starts to turn toward the LVOT from the mid-ventricle (Fig. 1b), and the vortices are seen evolving on both sides of the mitral valve (Fig. 1c). One or both of these vortices has been demonstrated to some extent by several other researchers (Kilner et al. 2000; Garcia et al. 2010; Cimino et al. 2012; Töger et al. 2012). The vortex behind the posterior mitral ring diminishes and disappears early, whereas the vortex in the LVOT persists and propagates toward the apex (Fig. 1c). The opposing flow directions in this vortex during early filling are also visible by conventional CDI and CMM and PW Doppler as peak early velocity in LVOT (E_{LVOT}). This flow is slightly delayed in relation to the mitral inflow (E) and the peak annular velocity (e'). This is demonstrated in Figure 2a and 2b, and time intervals are given in Table 3.

In diastasis the mid-ventricular vortex combines with the vortex in the LVOT, creating a large vortex that occupies most of the LV (Fig. 1d) (Garcia et al. 2010). The center of the vortex moves more apically during diastasis. With the start of the atrial contraction (A), there is further basal motion of the AV-plane, flow through the mitral valve increases again, and the same pattern is seen evolving as in early filling (Fig. 1e), again with delayed flow into the LVOT (Fig. 2). This has previously been described as the J-wave (Jaeger and Rahko 1990). The second vortex merges with the existing apical vortex, and during this phase it grows and moves more centrally in the LV. The vortex is centered right above the mitral valve and reaches from the basis to the apex of the LV.

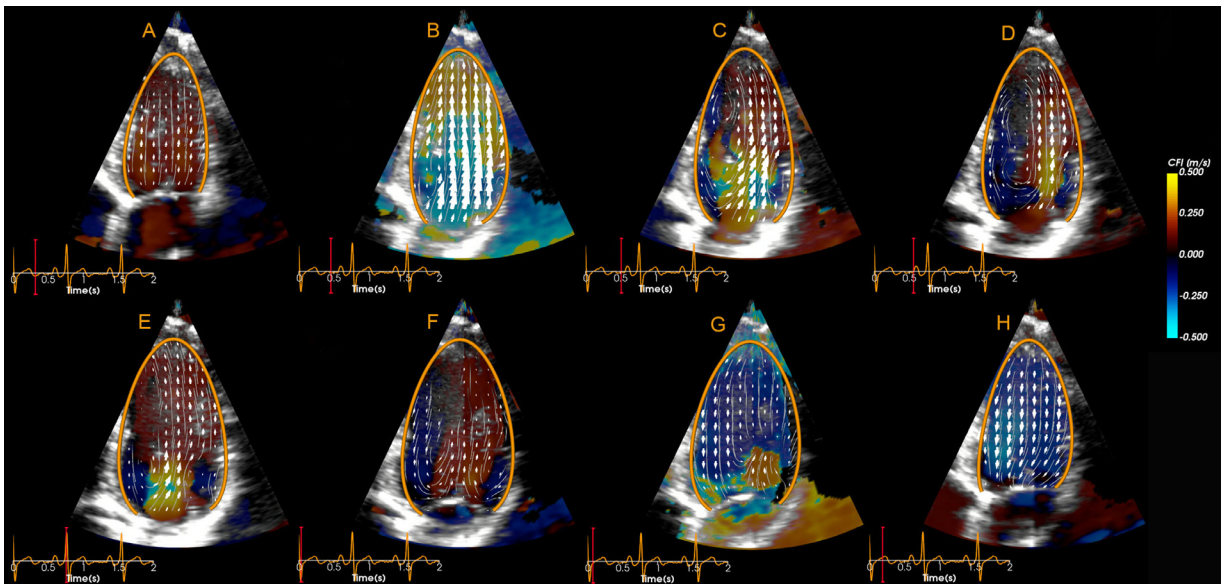

Fig. 1. Intraventricular vortices and flow visualized with blood speckle tracking (BST). Still images from eight different timepoints in the cardiac cycle, visualizing the most prominent vortex and flow patterns in the given phase. (a) Isovolumetric relaxation, showing flow toward the apex in the whole ventricle. (b) Early rapid filling (E-wave), showing reversal of flow due to basal movement can be seen in the mid-ventricle near the septum and left ventricular outflow. (c) Late rapid filling (E-wave), showing reversal of flow also near apex, generating a vortex in the whole length of the ventricle, persisting into (d) diastasis. (e) Atrial contraction (A-wave), showing the same pattern as the E-wave with flow reversal into the left ventricular outflow tract (LVOT). (f) Isovolumetric contraction, showing a vortex filling the ventricle, with apically directed flow in the lateral part and basally directed flow along the septum. (g) Early ejection, showing some persistence of the vortex, with apical flow laterally. (h) Late ejection, where no vortex can be seen.

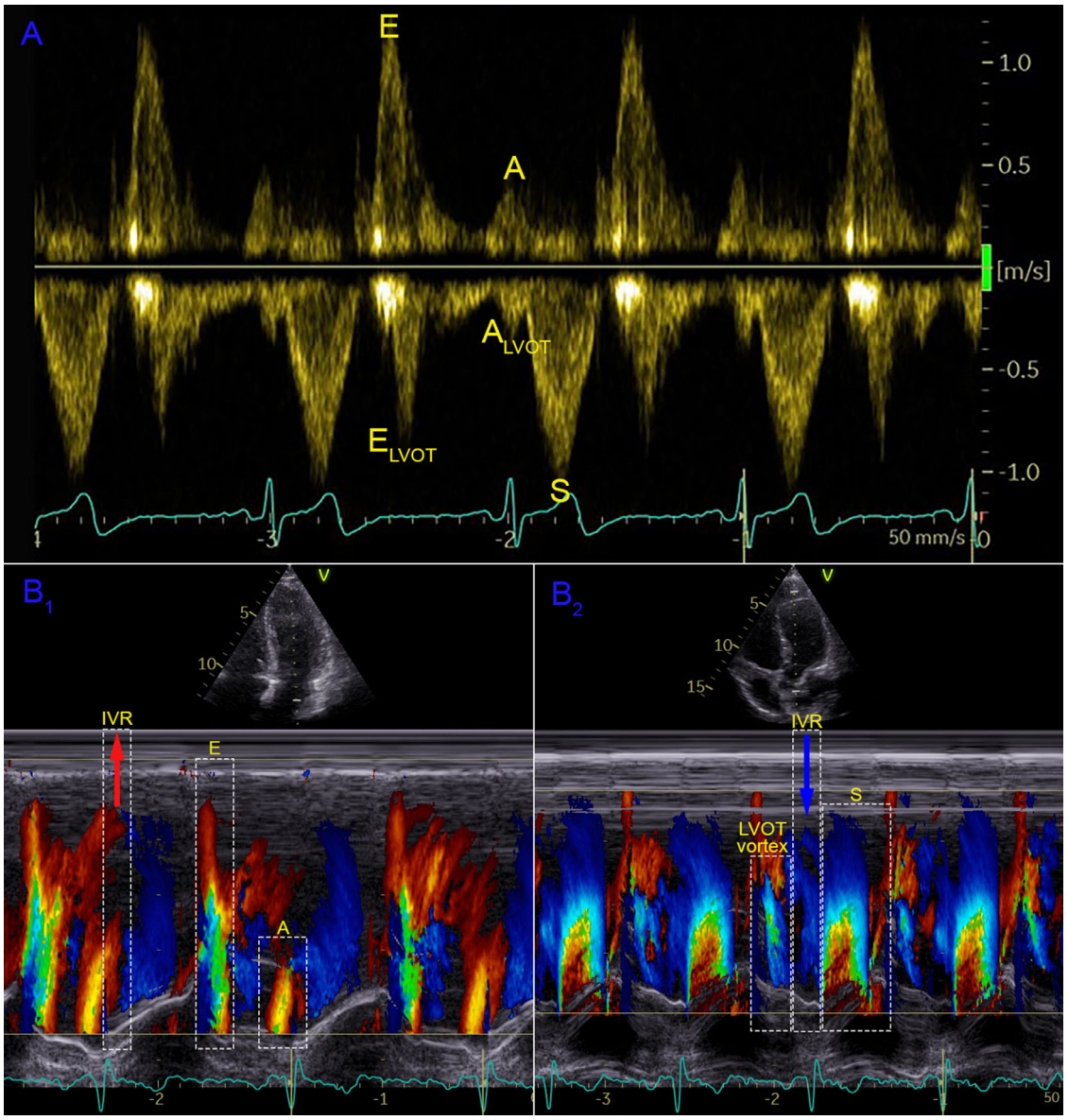

Fig. 2. Intraventricular vortices and flow visualized. (a) Pulsed-wave (PW) Doppler trace with sample volume between the mitral and aortic valve visualizing the E-wave, the A-wave and the delayed mirrored E-wave and A-wave in the opposite direction in the left ventricular outflow tract (LVOT). We also see the ejection (the S-wave). Apically directed flow can also be seen during IVR. (b) Color M-mode (CMM) recordings through the mitral valve and the LVOT, respectively. B_1: E-wave and A-wave and IVR-flow, all directed toward the apex. B_2: Shows the vortex in the LVOT, the S wave with direction toward the base and IVR-flow directed toward the apex.

This vortex may thus contribute to the closing of the mitral valve (Sherrid et al. 2017) and persists into the IVC (Li et al. 2019).

Table 3. Timing of flow and peak velocity (n = 21)

Time between R and peak mitral E (ms)	497 (481–528)
Time between R and peak septal e' (ms)	484 (434–513)
Time between R and peak LVOT E (ms)	613 (575–651)

Data are expressed as median (interquartile range) or number

E, early filling; e', early diastolic tissue velocity; LVOT, left ventricular outflow tract; R, the R in the QRS complex.

With both the mitral and the aortic valve closed, the flow will continue to swirl inside the LV (Fig. 1f). This pattern is also seen in CMM (Fig. 2b), showing a column of blood toward the apex along the lateral wall, and the opposite along the septum. As the aortic valve opens, this flow continues out through the open valve and into the aorta. The part of the blood in the LV that is not passing through the aortic valve is deflected and moved by the closed mitral valve and continues to conserve the vortex from the previous phase (Fig. 1g). As the flow out

of the LV increases, the AV-plane moves and the LV contracts, the vortex diminishes and moves toward the lateral wall. The vortex visually seems to dissolve in this phase (Fig. 1h), although the VO plot indicates persistence of part of the vortex through the whole heart cycle (Fig. 3).

Quantitative flow results

Detailed results of average values in diastole and systole of the experimental measurements of KE, rate of EL and VO are listed in Table 4. Figure 3 displays the KE trace, the ĖL trace and the VO trace from top to bottom and shows how the different parameters relate temporally to each other and to the ECG. KE have peaks at the same time as the peak flow. During the IVR, the KE begins to rise, peaking at peak E, which is consistent with the flow pattern described earlier during this phase. The same peaks occur at the E-wave and A-wave in the ĖL, but with a steeper rise and fall in the E-wave and a slightly delayed peak when compared with the KE. The ĖL depicts high values when the flow is high, but we also see a larger decline in the ĖL than in the KE after peak flow, indicating that the KE has less variations throughout the cardiac cycle than the ĖL. During the E-wave, the most complex blood flow is observed, and both Figures 3 and 4 show that the main ĖL is during this phase. The ĖL also falls to a lower level when compared to the peak values that we see in KE and VO. Peaks are shown at the E-wave and the A-wave in the

Table 4. Experimental quantitative measures (n = 21)

Mean KE diastole (J/m)	0.20 (0.17–0.23)
Mean KE systole (J/m)	0.21 (0.18–0.25)
Mean ĖL diastole (mW/m)	4.44 (3.41–5.44)
Mean ĖL systole (mW/m)	4.79 (2.79–6.49)
Mean VO diastole (Hz)	10.00 (9.15–11.07)
Mean VO systole (Hz)	8.55 (7.77–10.14)

Data are expressed as median (interquartile range)
EL, energy loss; KE, kinetic energy; VO, vorticity

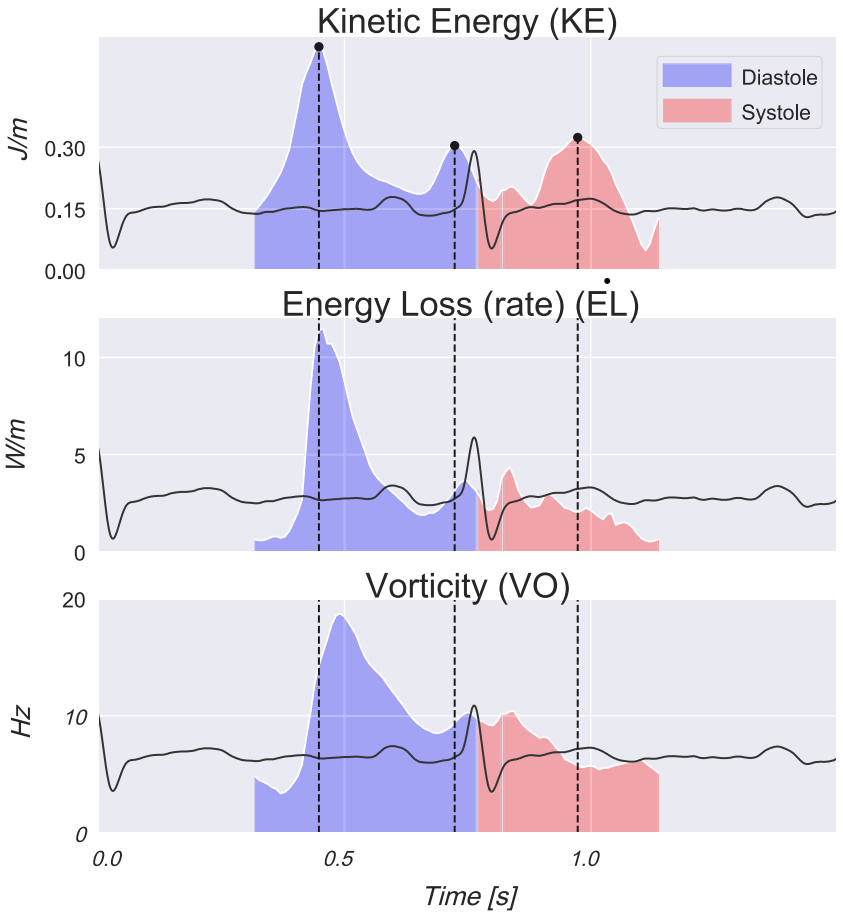

Fig. 3. Kinetic energy (KE), energy loss (rate) ($\dot{EL}$), and vorticity (VO) from one subject. Traces from one subject, matched in time at peak kinetic energy in the different phases, showing how the experimental measurements vary during the cardiac cycle and how they relate to each other. The lines correspond to the peaks of the KE at the E-wave, the A-wave and the ejection.

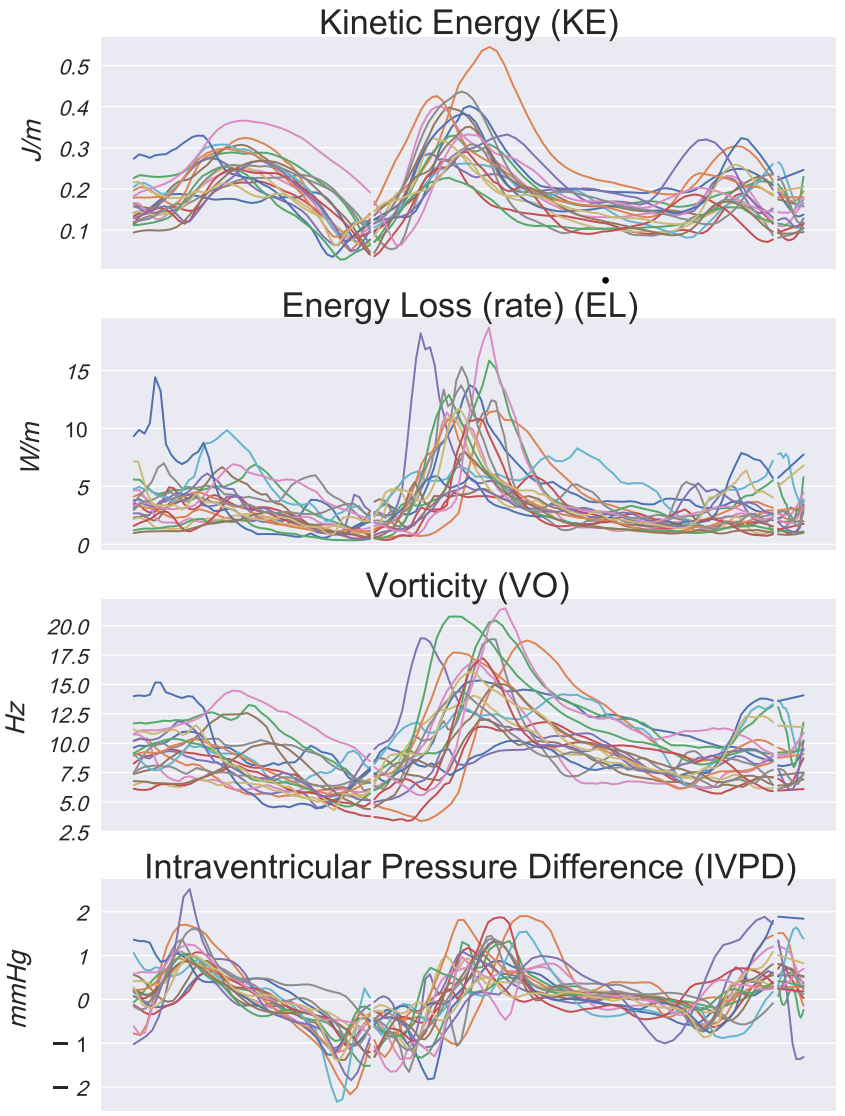

Fig. 4. Kinetic energy (KE), energy loss (rate) ($\dot{EL}$), vorticity (VO) and pressure difference (PD) from all subjects. Traces from all study subjects plotted together in one plot per measurement. The plots depict how the curves from the different subjects follow the same pattern even though the maximum and minimum values vary. The vertical lines through the curves mark the separation of the systole and the diastole, respectively.

VO, but with a delayed peak and a more protracted duration than KE, in concordance with the qualitative results seen by BST and described earlier.

Also note that the VO is declining during ejection, as anticipated when looking at the qualitative flow results. The vortex may be dissolving during this phase. For all the subjects, the trace showed the same pattern, although with different values, as is shown in Figure 4. The measurements are taken from an apical four-chamber view, and thus we can expect more accurate values for the parts related to the mitral flow (the diastolic part) than for the part related to the ejection (the systolic part) because the LVOT is not visualized in this view.

The trace of the IVPD from one of the subjects is shown in Figure 5a. From the start of this curve, the ejection out the aortic valve occurs as an acceleration of flow toward the base. As the flow slows, the pressure difference also declines. It shifts to a negative value when the flow decelerates as the ejection comes to an end. Then, during IVR, an acceleration begins toward the apex that continues into the rapid filling of the diastole. This corresponds to the low velocity flow seen with CDI in the IVR, as described in the section on qualitative flow results. After the rapid filling, flow decelerates and the pressure difference stabilizes around zero until a negative pressure difference again accelerates the flow toward the apex during atrial contraction.

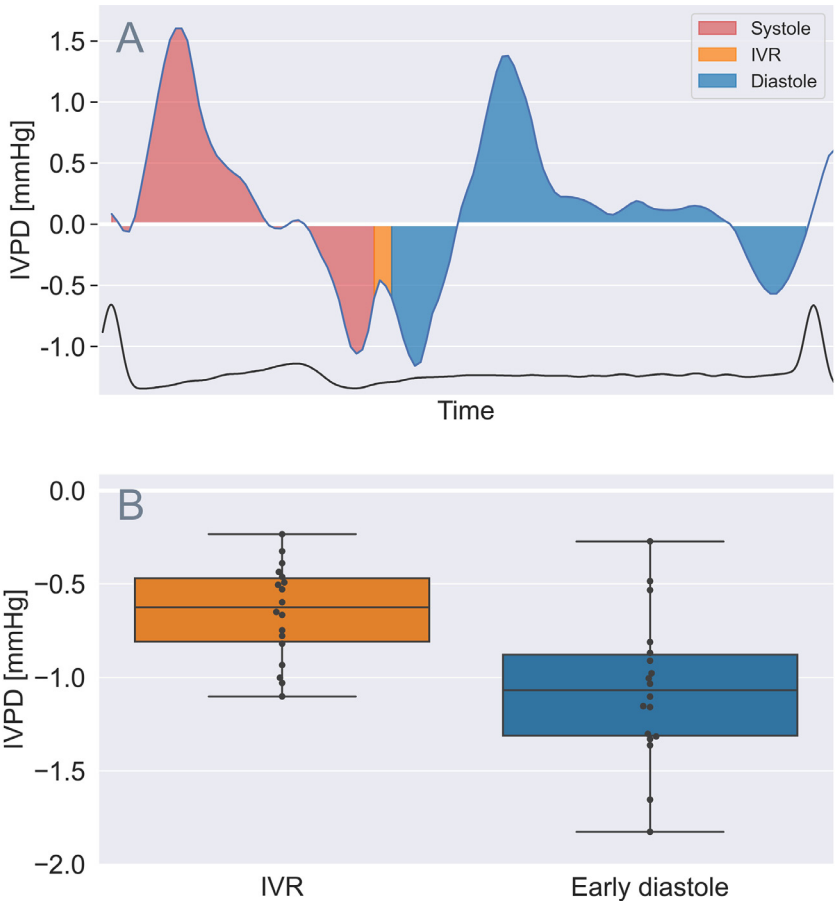

Fig. 5. Pressure differences. Figure A show an intraventricular pressure difference curve from one case throughout the cardiac cycle. Positive numbers depict pressure increase toward the apex, giving acceleration of basally directed blood flow, or deceleration of apically directed blood flow. Negative numbers depict pressure increase toward the base, giving acceleration of apically directed flow or deceleration of basally directed flow. From the start acceleration of ejection flow occurs toward the base out through the aortic valve, then deceleration of flow occurs as the ejection comes to an end. This means that in the last part of ejection, ejection flow is against a pressure gradient and must be inertia driven. During isovolumetric contraction (IVR) acceleration starts toward the apex that continues into the rapid filling of the diastole. During the latter part of early filling we again see a deceleration of flow, and inertially driven flow, and finally a stabilization of the pressure difference around zero during diastasis, with a new acceleration during atrial contraction. (b) A boxplot of the pressure differences from the isovolumetric relaxation (IVR) period and early diastole, showing that the pressure gradient is considerably higher during rapid filling.

Figure 5b shows that the IVPD from the IVR and the early diastole both indicate an acceleration of flow toward the apex. The pressure difference in IVR is lower than in the early ejection, showing that the flow starts to accelerate during the IVR and picks up as the mitral valve opens for the rapid inflow.

DISCUSSION

This study evaluated the normal LV intraventricular flow patterns with a very high temporal resolution. Intraventricular VFI with BST provides a more detailed visualization of the intracardiac flow than CDI alone. This study shows that BST is feasible in healthy adults down to a depth of approximately 10−12 cm, visualizing intraventricular flow with high temporal resolution. The extraction of quantitative measures such as VO, KE, ĖLand IVPD is also feasible. This study also demonstrated vortex formation in relation to the different phases of the heart cycle and in relation to wall motion and deformation.

Intraventricular flow seems to originate during IVR (Fig. 1a), where an elongation of the apex and a simultaneous shortening of the base can be seen with strain rate, although a remaining apically directed part of the vortex may contribute as well. The elongation of the apex is possibly related to the apical untwisting previously demonstrated with both magnetic resonance and echocardiography (Rademakers et al. 1992; Takeuchi et al. 2006).

This generates an intraventricular pressure gradient (Nikolic et al. 1995; Cimino et al. 2012) and subsequent flow toward the apex (Sasson et al. 1987; Garcia et al. 2010), even with the valves closed. Thus, myocardial work by shortening of the base, despite concomitant elongation of the apex, is not "wasted work," but is instrumental in initiating the apical momentum of the blood. Using the high-frame-rate imaging setup, we were able to both resolve this flow by CDI and to measure the pressure gradient from BST. The intraventricular flow created in IVR presumably facilitates early filling through the momentum created. From the IVPD curves, flow accelerates smoothly from the IVR into the early filling, which also supports this finding. Hodzic et al. (2020) recently demonstrated that CDI-derived peak early diastolic IVPD provides a reliable flow-based index of early left ventricular diastolic function, supporting our findings that this start of flow is important for optimal cardiac function.

As blood flows into the LV from the left atrium, the chamber diameter of the LV is larger than the diameter of the mitral orifice. Basic physical mechanisms tell us that this alone will create vortices because the blood will need to fill the LV. At the same time, the AV-plane moves basally, expanding the space where there is no direct inflow from the atrium. This creates a suction that in turn will divert some of the blood back toward the base, causing vortex formation. As the LV is asymmetrical with a larger space behind the anterior mitral leaflet than the posterior leaflet, the vortex will be asymmetrical, and the lateral vortex appears short-lived. These two vortices have been shown earlier by several research groups (Garcia et al. 2010; Cimino et al. 2012; Töger et al. 2012; Khalafvand et al. 2017).

Simultaneous with the development of the septal and lateral vortices, a rapid flow propagation occurs toward the apex and a trailing vortex develops. This trailing vortex starts at LV mid-level (Fig. 1b) and not in the apex, as has been previously described (Cimino et al. 2012). This vortex will still remain some time before combining with the septal vortex to create one large vortex in the whole of the LV (Fig. 1d). Thus, the first blood to reach the apex is the rapid flow propagation, followed by the slower vortex. This phenomenon has already been shown with CMM and CDI by Rodevand et al. (1999) and Steen and Steen (1994). The pattern during the E-wave and the A-wave are similar, but the velocity of the flow will affect the vortex development. Therefore, differences will be seen in the E/A pattern according to the normal shift in E/A-configuration with age, and these differences will be translated to the patterns seen in the LVOT as well.

After both the E-wave and the A-wave, the flow persists in one large vortex, and as this vortex continues into the IVC (Fig. 1f) it is reasonable to assume that this maintains the momentum and the KE of the blood into the systole. When the aortic valve opens, the movement of the blood flow inside the LV is already well aligned along the septum toward the basis. With the start of the systole, the flow already has momentum and can thus continue unhindered into the aorta. The momentum will contribute to overcoming the aortic pressure, thus reducing afterload. In the early part of systole, we still observe some of the blood flow diverging at the basis and following the lateral wall toward the apex again (Fig. 1g), but during ejection this flow decreases (Fig. 1h).

The observations with CDI and vector plots show no consistent sign of a persistent systolic vortex in all subjects, although there is persistent VO in the quantitative results and a negative IVPD after acceleration of systolic flow. Both findings suggest that there might be a deviation of flow at the AV-plane also after the aortic valve has closed. This might be the start of the apically directed flow in the IVR and thus a conservation of momentum into this phase. Further studies are needed to investigate this phenomenon in more detail.

Our results give a detailed description of the intraventricular flow in the LV throughout the whole cardiac cycle. A few earlier studies have shown the flow throughout the cardiac cycle, but not with direct measurement of the flow direction and not with the same frame rate. Garcia et al. (2010) used frame interleaving from 8−12 beats to increase temporal resolution of CDI in an interpolated, merged cycle of 200 frames. Cimino et al. (2012) had a frame rate of 80 Hz with echo-PIV, although measures are taken to improve frame rate in echo-PIV (Voorneveld et al. 2019). Most of the earlier research done has looked at only parts of the cardiac cycle, meaning that the interaction between the different parts of the cycle, and which phenomena that link and follow each other, is not fully explained. Also, with the high temporal resolution of 4 ms obtained with our method, this short-lived phenomenon can be studied.

The KE, ĖL and VO seem to follow the same pattern as the flow in the ventricle. This is best visible for the E-wave in Figure 3 because the subject is a younger person. We also see that the rise in KE starts in the IVR, which again supports our finding that the apically directed flow starts during IVR. Figures 3 and 4 show that the main ĖL is during the E-wave when the most complex blood flow and the highest velocities are observed. Further studies with patients are required to see whether the complexity of the blood flow might be linked to the ĖL. The high relative values of the ĖL also indicate that a large potential exists for increasing EL if the blood flow pattern starts deviating from normal, even though the absolute values measured here are very low when compared with the total work of the heart. The impact of the forces on the cardiac function is not

obvious, and further clinical research is needed to examine the clinical value.

The VO shows high values during the phases in the cardiac cycle when the best visible vortex patterns qualitatively are observed. Figure 3 shows that the VO peaks a bit later than the KE when the rapid inflow column of blood has reached the apex and the vortices described in the results section are most visible. As the vortices combine throughout the diastasis the VO falls, as expected. A small rise again occurs when the atrial contraction happens, with the formation of new vortices. This coincides with the results from Faurie et al. (2017, 2019), showing two main peaks in the VO curves slightly delayed when compared with the E-wave and A-wave. They also observed a relationship between the tissue and the vortex waveforms, also with a slight delay, denoting the lag between the wall and the flow motion. Then, during ejection, the VO falls as time goes on, but notably not to zero. This indicates that there is some movement of blood, and maybe some vortices, during the late phases of systole, even though no certain vortices have been observed in this phase.

The clinical interpretation of the quantitative measures is unclear and must be evaluated in relation to pathologic ventricles in future clinical studies. Both the values of the measurements and the shape of the curves can potentially be used to differentiate between healthy and diseased ventricles. Values extracted with other methods will most likely result in different values because of different technology and post-processing, and the future will show whether they will be comparable.

Duplex (B-mode with CDI) frame rate lies between 20 and 30 frames/s and thus results in a temporal resolution of 40 ms. For the short-lived isovolumetric phases, a mean duration of 57 ms (IVR) and 35 ms (IVC) is shown in our material. With the duplex frame rate this means that we will have maximum one frame during IVC. With a frame rate of 250 Hz, which is approximately what was obtained in these experimental data, a temporal resolution of 4 ms was achieved, making it possible to study short-lived phases and phenomena in more detail. CMM is the only conventional acquisition that can obtain a frame rate similar to our data and is therefore used as 1-D reference for parts of our results (Fig. 2b). The real clinical need for a high frame rate will only be evident after we know what can be seen with a high frame rate that is not apparent at a lower frame rate; thus, more research on the topic is required.

Strengths and Limitations

The method yields a high frame rate and a very high temporal resolution that makes studying short-lived phenomena feasible. With a frame rate of 250 Hz, a temporal resolution of 4 ms is achieved, whereas at 50 Hz only a temporal resolution of 20 ms is achieved.

The participant group was selected and was mostly young and echogenic. Thus, the true feasibility in an older population is unclear.

Images are stitched over five to six cycles, which means that the technology cannot be used in patients with conditions as atrial fibrillation or frequent extra systoles.

The visualization of the flow is sensitive to view; small changes from the standard view may change the absolute flow velocities that we measure, although the qualitative interpretation is mostly still available.

Model-based regularization can in some cases show flow patterns that are not real. This is compensated for by weighing in measured data from speckle tracking and by making sure that the flow pattern matches the CDI pattern.

In most cases, the images were obtained during breath hold to get a stable image. Breath hold can contribute to changes in the normal physiology. Breath hold for six heart cycles is also less feasible in older subjects with heart disease, so acquisition during quiet respiration instead must be demonstrated to be adequate.

High-frame-rate and raw (in-phase and quadrature) data produce very large files, which is demanding regarding data transfer and storage.

The images are obtained as a 3-D slice but are analyzed in 2-D. The 10-degree thickness of the 3-D slice is used to estimate out-of-plane motion to improve the flow in the 2-D images, but a full 3-D volume is preferable to correctly visualize intracardiac flow. Unfortunately, the full 3-D-volumes do not get high enough frame rate as of when this study was published.

Future perspectives

This study has described a normal pattern of the complex blood flow inside the LV. The next step in evaluating this method will be to investigate potential differences in flow pattern and the quantitative measurements in patients with deviating geometry of the LV to see if this method can be an addition in the evaluation and treatment of patients with different heart diseases.

CONCLUSIONS

This study demonstrates that VFI with BST technology is feasible in healthy adults down to a depth of 10−12 cm. The thick-slice method allows flexible retrospective analysis including vector plots as an important supplement for better visualization of the blood flow without using a contrast agent.

The geometry of the LV and the piston-like movement of the AV-plane is important in creating vortices

that are favorable for blood flow and facilitate outflow. The investigation of these complex blood flow patterns may yield new information about the LV function, both regarding physiology and pathology, and can potentially supplement the treatment of patients with varying heart diseases.

Acknowledgments—A.S. Daae and S. Fadnes are funded by the Liaison Committee for education, research and innovation in Central Norway. M.S. Wigen is funded by Centre for Innovative Ultrasound Solution (CIUS). CIUS is a Centre for Research-based Innovation (SFI) appointed by the Research Council of Norway for the period from 2015 to 2023. GE Vingmed Ultrasound AS is a partner in CIUS.

Conflict of interest disclosure—A.S. Daae, M.S. Wigen, S. Fadnes and A. Støylen have no conflicts of interest to state. L. Løvstakken is a part time consultant for GE Vingmed Ultrasound AS.

SUPPLEMENTARY MATERIALS

Supplementary material associated with this article can be found in the online version at doi:10.1016/j.ultrasmedbio.2021.08.021.

APPENDIX

The quantitative parameters summarize different flow features and can shed light on different physiologic aspects. The definitions used in this paper are as follows:

Kinetic energy (KE)

The KE of the blood is the energy the blood possesses owing to its motion. The KE per unit volume of fluid q is given by

$$q = \frac{1}{2}\rho v^2, \tag{1}$$

where $\rho = 1060$ kg/m^3 is the density of the blood and v is the velocity magnitude. Since we do not have full volumetric data, we integrate over a 2-D region (the left ventricle [LV]), to retrieve the KE time trace with the resulting unit of J/m.

$$KE = \int q\, dA \tag{2}$$

Energy loss (EL)

The EL is related to the viscous losses of the fluid. This is determined by the shear forces and intrinsic fluid velocity and is a 3-D measurement. In 2-D we assume only planar shear forces and integrate over the area. The rate of energy loss is given by the equation

$$\dot{EL} = \mu \int 2\left(\frac{\partial v_x}{\partial x}\right)^2 + 2\left(\frac{\partial v_y}{\partial y}\right)^2 + \left(\frac{\partial v_x}{\partial y} + \frac{\partial v_y}{\partial x}\right)^2 dA, \tag{3}$$

where $v = [v_x, v_y]$ is the blood velocity vector and $\mu = 0.004$ Pa·s is the blood viscosity. The unit of $\dot{EL}$ when integrated over a two-dimensional region is W/m. Using a time integral, the energy loss EL [J/m] over a given time period can be extracted.

Vorticity (VO)

The VO is a measure of the rotation of the blood around each point in the image at one timepoint in the cardiac cycle and is a measure of the complexity of the blood flow. It is calculated by the curl or momentum of the blood velocity field. It is given by the equation

$$VO = \left| \underset{\omega}{\rightarrow} \right| = \left| \frac{\partial v_y}{\partial x} - \frac{\partial v_x}{\partial y} \right| \tag{4}$$

The unit of VO is Hz. The resulting time trace of VO is found by averaging the region of interest (the LV).

Intraventricular pressure differences (IVPD)

The pressure gradient is estimated from the velocity field as follows:

$$\frac{\partial P}{\partial x} = -\rho\left(\frac{\partial v_x}{\partial t} + v_x\frac{\partial v_x}{\partial x} + v_y\frac{\partial v_x}{\partial y}\right) + \mu\,\nabla^2 v_x, \tag{5}$$

$$\frac{\partial P}{\partial y} = -\rho\left(\frac{\partial v_y}{\partial t} + v_y\frac{\partial v_y}{\partial y} + v_x\frac{\partial v_y}{\partial x}\right) + \mu\,\nabla^2 v_y, \tag{6}$$

where $\rho = 1060$ kg/m^3 is the density of the blood, $v = [v_x, v_y]$ is the blood velocity vector and $\mu = 0.004$ Pa/s is the blood viscosity. IVPD is found by integrating the pressure gradients along a manually defined path in the LV from base to apex. The path is a spline curve defined by three or more points set by the user according to the mitral inflow streamlines.

$$IVPD = \int \frac{\partial P}{\partial x}dx + \int \frac{\partial P}{\partial y}dy \tag{7}$$

The path is static, meaning that the length and position stays the same during the cardiac cycle. Thus, the measurements are most accurate for the timepoint where the path was drawn, as the path will not follow the movement of the AV plane, or the walls of the LV. Positive numbers depict acceleration of blood toward the base or deceleration of flow when the blood has a direction toward the apex. Negative numbers depict acceleration of blood toward the apex or deceleration of flow when the blood has a direction toward the basis. The unit of IVPD is millimeters of mercury (mm Hg).

REFERENCES

Akiyama K, Maeda S, Matsuyama T, Kainuma A, Ishii M, Naito Y, Kinoshita M, Hamaoka S, Kato H, Nakajima Y, Nakamura N, Itatani K, Sawa T. Vector flow mapping analysis of left ventricular

energetic performance in healthy adult volunteers. BMC Cardiovasc Disord 2017;17:21.
Arvidsson PM, Töger J, Heiberg E, Carlsson M, Arheden H. Quantification of left and right atrial kinetic energy using four-dimensional intracardiac magnetic resonance imaging flow measurements. J Appl Physiol (1985) 2013;114:1472–1481.
Bellhouse BJ. Fluid mechanics of a model mitral valve and left ventricle. Cardiovascular research 1972;6:199–210.
Bohs LN, Friemel BH, Kisslo J, Harfe DT, Nightingale KR, Trahey GE. Three-dimensional flow images by reconstruction from two-dimensional vector velocity maps. J Am Soc Echocardiogr 1995;8:915–923.
Bot H, Verburg J, Delemarre BJ, Strackee J. Determinants of the occurrence of vortex rings in the left ventricle during diastole. J Biomech 1990;23:607–615.
Cimino S, Pedrizzetti G, Tonti G, Canali E, Petronilli V, De Luca L, Iacoboni C, Agati L. In vivo analysis of intraventricular fluid dynamics in healthy hearts. Eur J Mechan B Fluids 2012;35:40–46.
Demené C, Deffieux T, Pernot M, Osmanski BF, Biran V, Gennisson JL, Sieu LA, Bergel A, Franqui S, Correas JM, Cohen I, Baud O, Tanter M. Spatiotemporal clutter filtering of ultrafast ultrasound data highly increases Doppler and ultrasound sensitivity. IEEE Trans Med Imaging 2015;34:2271–2285.
Elbaz MS, van der Geest RJ, Calkoen EE, de Roos A, Lelieveldt BP, Roest AA, Westenberg JJ. Assessment of viscous energy loss and the association with three-dimensional vortex ring formation in left ventricular inflow: In vivo evaluation using four-dimensional flow MRI. Magn Reson Med 2017;77:794–805.
Fadnes S, Sørensen K, Nyrnes SA, Wigen MS, Lovstakken L. Intraventricular pressure gradients: Vector flow imaging versus color M-mode. Proc IEEE Int Ultrason Symp (IUS) 2020;1–4.
Fadnes S, Wigen MS, Nyrnes SA, Lovstakken L. In vivo intracardiac vector flow imaging using phased array transducers for pediatric cardiology. IEEE Trans Ultrason Ferroelectr Freq Control 2017;64:1318–1326.
Faurie J, Baudet M, Assi KC, Auger D, Gilbert G, Tournoux F, Garcia D. Intracardiac vortex dynamics by high-frame-rate Doppler vortography-in vivo comparison with vector flow mapping and 4-D flow MRI. IEEE Trans Ultrason Ferroelectr Freq Control 2017;64:424–432.
Faurie J, Baudet M, Poree J, Cloutier G, Tournoux F, Garcia D. Coupling myocardium and vortex dynamics in diverging-wave echocardiography. IEEE Trans Ultrason Ferroelectr Freq Control 2019;66:425–432.
Fenster BE, Browning J, Schroeder JD, Schafer M, Podgorski CA, Smyser J, Silveira LJ, Buckner JK, Hertzberg JR. Vorticity is a marker of right ventricular diastolic dysfunction. Am J Physiol Heart Circ Physiol 2015;309:H1087–H1093.
Garcia D, Del Alamo JC, Tanne D, Yotti R, Cortina C, Bertrand E, Antoranz JC, Perez-David E, Rieu R, Fernandez-Aviles F, Bermejo J. Two-dimensional intraventricular flow mapping by digital processing conventional color-Doppler echocardiography images. IEEE Trans Med Imaging 2010;29:1701–1713.
Grønli T, Wigen M, Segers P, Lovstakken L. A fast 4D B-spline framework for model-based reconstruction and regularization in vector flow imaging. IEEE Int Ultrason Symp 2018;1–9.
Hodzic A, Garcia D, Saloux E, Ribeiro PAB, Ethier A, Thomas JD, Milliez P, Normand H, Tournoux F. Echocardiographic evidence of left ventricular untwisting-filling interplay. Cardiovasc Ultrasound 2020;18:8.
Hong GR, Pedrizzetti G, Tonti G, Li P, Wei Z, Kim JK, Baweja A, Liu S, Chung N, Houle H, Narula J, Vannan MA. Characterization and quantification of vortex flow in the human left ventricle by contrast echocardiography using vector particle image velocimetry. JACC Cardiovasc Imaging 2008;1:705–717.
Jaeger KM, Rahko PS. Doppler characteristics of late-diastolic flow in the left ventricular outflow tract. J Am Soc Echocardiogr 1990;3:179–186.
Jensen JA, Nikolov SI, Yu AC, Garcia D. Ultrasound vector flow imaging-part I: Sequential systems. IEEE Trans Ultrason Ferroelectr Freq Control 2016a;63:1704–1721.
Jensen JA, Nikolov SI, Yu AC, Garcia D. Ultrasound vector flow imaging-part II: Parallel systems. IEEE Trans Ultrason Ferroelectr Freq Control 2016b;63:1722–1732.
Kanski M, Arvidsson PM, Töger J, Borgquist R, Heiberg E, Carlsson M, Arheden H. Left ventricular fluid kinetic energy time curves in heart failure from cardiovascular magnetic resonance 4D flow data. J Cardiovasc Magn Reson 2015;17:111.
Khalafvand SS, Ng EYK, Zhong L, Hung TK. Three-dimensional diastolic blood flow in the left ventricle. J Biomech 2017;50:71–76.
Kilner PJ, Yang GZ, Wilkes AJ, Mohiaddin RH, Firmin DN, Yacoub MH. Asymmetric redirection of flow through the heart. Nature 2000;404:759–761.
Kim WY, Walker PG, Pedersen EM, Poulsen JK, Oyre S, Houlind K, Yoganathan AP. Left ventricular blood flow patterns in normal subjects: A quantitative analysis by three-dimensional magnetic resonance velocity mapping. J Am Coll Cardiol 1995;26:224–238.
Li Q, Huang L, Ma N, Li Z, Han Y, Wu L, Zhang X, Li Y, Zhang H. Relationship between left ventricular vortex and preejectional flow velocity during isovolumic contraction studied by using vector flow mapping. Echocardiography 2019;36:558–566.
Mehregan F, Tournoux F, Muth S, Pibarot P, Rieu R, Cloutier G, Garcia D. Doppler vortography: A color Doppler approach to quantification of intraventricular blood flow vortices. Ultrasound Med Biology 2014;40:210–221.
Nagueh SF, Smiseth OA, Appleton CP, Byrd BF, 3rd, Dokainish H, Edvardsen T, Flachskampf FA, Gillebert TC, Klein AL, Lancellotti P, Marino P, Oh JK, Alexandru Popescu B, Waggoner AD. Recommendations for the evaluation of left ventricular diastolic function by echocardiography: An update from the American Society of Echocardiography and the European Association of Cardiovascular Imaging. Eur Heart J Cardiovasc Imaging 2016;17:1321–1360.
Nakashima K, Itatani K, Kitamura T, Oka N, Horai T, Miyazaki S, Nie M, Miyaji K. Energy dynamics of the intraventricular vortex after mitral valve surgery. Heart Vessels 2017;32:1123–1129.
Nikolic SD, Feneley MP, Pajaro OE, Rankin JS, Yellin EL. Origin of regional pressure gradients in the left ventricle during early diastole. Am J Physiol 1995;268:H550–H557.
Nyrnes SA, Fadnes S, Wigen MS, Mertens L, Lovstakken L. Blood speckle-tracking based on high-frame rate ultrasound imaging in pediatric cardiology. J Am Soc Echocardiogr 2020;33:493–503 e5.
Pedrizzetti G, La Canna G, Alfieri O, Tonti G. The vortex—an early predictor of cardiovascular outcome?. Nat Rev Cardiol 2014;11:545–553.
Rademakers FE, Buchalter MB, Rogers WJ, Zerhouni EA, Weisfeldt ML, Weiss JL, Shapiro EP. Dissociation between left ventricular untwisting and filling. Accentuation by catecholamines. Circulation 1992;85:1572–1581.
Rodevand O, Bjornerheim R, Edvardsen T, Smiseth OA, Ihlen H. Diastolic flow pattern in the normal left ventricle. J Am Soc Echocardiogr 1999;12:500–507.
Sasson Z, Hatle L, Appleton CP, Jewett M, Alderman EL, Popp RL. Intraventricular flow during isovolumic relaxation: Description and characterization by Doppler echocardiography. J Am Coll Cardiol 1987;10:539–546.
Sherrid MV, Kushner J, Yang G, Ro R. Mitral valve coaptation and its relationship to late diastolic flow: A color Doppler and vector flow map echocardiographic study in normal subjects. Echocardiography 2017;34:537–548.
Steen T, Steen S. Filling of a model left ventricle studied by colour M mode Doppler. Cardiovasc Res 1994;28:1821–1827.
Takeuchi M, Nakai H, Kokumai M, Nishikage T, Otani S, Lang RM. Age-related changes in left ventricular twist assessed by two-dimensional speckle-tracking imaging. J Am Soc Echocardiogr 2006;19:1077–1084.
Töger J, Kanski M, Carlsson M, Kovács SJ, Söderlind G, Arheden H, Heiberg E. Vortex ring formation in the left ventricle of the heart: Analysis by 4D flow MRI and Lagrangian coherent structures. Ann Biomed Eng 2012;40:2652–2662.
Van Cauwenberge J, Lovstakken L, Fadnes S, Rodriguez-Morales A, Vierendeels J, Segers P, Swillens A. Assessing the performance of ultrafast vector flow imaging in the neonatal heart via multiphysics

modeling and in vitro experiments. IEEE Trans Ultrason Ferroelectr Freq Control 2016;63:1772–1785.

Voorneveld J, Keijzer LBH, Strachinaru M, Bowen DJ, Goei JSL, Ten Cate F, van der Steen AFW, de Jong N, Vos HJ, van den Bosch AE, Bosch JG. High-frame-rate echo-particle image velocimetry can measure the high-velocity diastolic flow patterns. Circ Cardiovas Imaging 2019;12 e008856.

Wang Y, Ma R, Ding G, Hou D, Li Z, Yin L, Zhang M. Left ventricular energy loss assessed by vector flow mapping in patients with prediabetes and type 2 diabetes mellitus. Ultrasound Med Biol 2016;42:1730–1740.

Wigen MS, Fadnes S, Rodriguez-Molares A, Bjastad T, Eriksen M, Stensaeth KH, Stoylen A. Lovstakken L. 4D intracardiac ultrasound vector flow imaging: Feasibility and comparison to phase-contrast MRI. IEEE Trans Med Imaging 2018;37:2619–2629.

Xu L, Sun C, Zhu X, Liu W, Ta S, Zhao D, Wang F, Liu L. Characterization of left ventricle energy loss in healthy adults using vector flow mapping: Preliminary results. Echocardiography 2017;34:700–708.

Yu A, Lovstakken L. Eigen-based clutter filter design for ultrasound color flow imaging: A review. IEEE Trans Ultrason Ferroelectr Freq Control 2010;57:1096–1111.

Zhong Y, Liu Y, Wu T, Song H, Chen Z, Zhu W, Cai Y, Zhang W, Bai W, Tang H, Rao L. Assessment of left ventricular dissipative energy loss by vector flow mapping in patients with end-stage renal disease. J Ultrasound Med 2016;35:965–973.